Desalination and Water Treatment
www.deswater.com

doi: 10.5004/dwt.2020.25061

180 (2020) 254–264
March

Investigation of simultaneous removal of fluoride and copper by induced crystallization using phosphate rock as a seed crystal

Linyu Deng[a,b,c,*], Ying Wang[a,b,c], Jianqi Zhou[a,b,c], Tinglin Huang[a,b,c], Xin Sun[a,b,c]

[a]*School of Environmental and Municipal Engineering, Xi'an University of Architecture and Technology, Xi'an 710055, China, Tel./Fax: +86-29-82202729; emails: denglinyu@xauat.edu.cn (L. Deng), ying_wangjiayou@163.com (Y. Wang), 810872857@qq.com (J. Zhou), huangtinglin@xauat.edu.cn (T. Huang), xinsunn@163.com (X. Sun)*
[b]*Key Laboratory of Northwest Water Resources, Environment and Ecology, Ministry of Education, Xi'an University of Architecture and Technology, Xi'an 710055, China*
[c]*Shaanxi Key Laboratory of Environmental Engineering, Xi'an University of Architecture and Technology, Xi'an 710055, China*

Received 30 March 2019; Accepted 22 October 2019

ABSTRACT

In this study, the simultaneous removal of F^- and Cu^{2+} based on an induced crystallization mechanism using phosphate rock as a seed crystal was investigated. F^- and Cu^{2+} could be effectively removed simultaneously until seed crystal phosphate rock (PR) was reused three times, but high Cu^{2+} levels lead to more residual F^- when the operations were performed more than three times. F^- was removed by induced crystallization of $Ca_{10}(PO_4)_6F_2$ on the surface of PR, and Cu^{2+} was removed by co-precipitation with $Ca_{10}(PO_4)_6F_2$ as $Ca_{10-x}(Cu)_x(PO_4)_6F_2$ on PR. The retarding effect of Cu^{2+} on the removal of F^- may be explained as being due primarily to the obstruction by Cu^{2+} to the deposition of lattice ion Ca^{2+} on the surface of PR, hence, this hindered the induced crystallization of $Ca_{10}(PO_4)_6F_2$. For an artificial multiple contaminants groundwater application, the concentration of F^- was decreased from 2.88 to 0.9 mg L^{-1} while the other heavy metals (Cu^{2+}, Zn^{2+} and Pb^{2+}) were all removed absolutely with additional P to reach a P:F ratio of 6:1 and a contact time of 1 h. These findings highlight the application of induced crystallization for the removal of multiple pollutants, including F^- and typical heavy metal ions, from groundwater.

Keywords: Fluoride; Heavy metals; Phosphate rock; Induced crystallization; Co-precipitation

1. Introduction

Fluoride (F^-) in groundwater (with the limit of 1.0 mg L^{-1}) [1] improves skeletal and dental health in humans but excess intake can lead to enzyme activity disorders, a metabolic imbalance of calcium and phosphorus, dental plaque, and joint deformation [2–4]. The F^- in F^--containing ores (CaF_2, Na_3AlF_6, and $Ca_{10}(PO_4)_6F_2$) get transported into the natural water [5]; in addition, many F^--containing wastewater is discharged into natural water through metal processing, aluminum electrolysis, glass and semiconductor manufacturing and phosphate production [6–9]. Therefore, excessive F^- levels (>1.0 mg L^{-1}) in groundwater are a problem worldwide. Su et al. [10] reported that the concentration of F^- in groundwater can be as high as 8.3 mg L^{-1} in the Datong Basin, North China. Narsimha and Sudarshan [11] also reported concentrations of F^- of 7.4 mg L^{-1} in Telangana, South India. Mirzabeygi et al. [12] reported F^- at 5.6 mg L^{-1} in Yazd, Iran.

Excess F^- often co-exists with heavy metals in groundwater [13–19]. Copper ion (Cu^{2+}) is a particularly harmful

* Corresponding author.

heavy metal; this is especially true for water ecosystems because it can readily accumulate to induce irreversible pollution and accumulation in the human body [20]. The limit of Cu^{2+} concentration is 1.0 mg L^{-1} according to the Chinese acceptable standards for drinking water [1]. Thus, it is often necessary to remove Cu^{2+} from groundwater.

Materials such as porous gelatin/acrylic acid, novel porous gelatin-silver/AcA [20], and phosphate rock (PR) [21] can serve as adsorbents to remove Cu^{2+} in water. In one study, the removal rate of Cu^{2+} was over 90% when PR was used as an adsorbent in solutions with less than 30 mg L^{-1} of Cu^{2+} [21]. The Cu^{2+} immobilization by PR was attributed to chemisorption, surface adsorption and complexation [22].

Our previous research showed that the F^- can be removed from 9.5 to 0.6 mg L^{-1} by induced crystallization using PR as a seed crystal [23]. Adding a quantitative PR seed crystal and precipitating agents (PO_4^{3-} and Ca^{2+}) to the F^- solutions in order to control the crystallization of the inorganic substances ($Ca_{10}(PO_4)_6F_2$) proceeded under the condition of supersaturation. The $Ca_{10}(PO_4)_6F_2$ is formed on the PR surface and gradually grew. Shanmugam et al [24]. reported that $Ca_{10-x}(Cu)_x(PO_4)_6F_2$ (x = 0.05–2.0) is formed when F^-, PO_4^{3-}, Ca^{2+}, and Cu^{2+} appeared in the solution concurrently. Thus, we inferred that the simultaneous removal of F^- and Cu^{2+} by PR could be achieved through two pathways: (1) the formation of $Ca_{10-x}(Cu)_x(PO_4)_6F_2$ (x = 0.05–2.0) on PR; and (2) the formation of $Ca_{10}(PO_4)_6F_2$ on PR in the solution. However, it is difficult to quantify the significance of the two mechanisms because they may act cooperatively. As such, the contribution of each mechanism should be determined.

The purpose of this study was to use PR as seed crystals to remove F^- and Cu^{2+} concurrently. The impacts of the Ca:P:F molar ratio, the reaction time, and the concentration of humic acid (HA) were investigated. The optimized conditions of the experiments were determined. The kinetics was modeled, and the reaction rates were calculated. The mechanisms of the co-removal of F^- and Cu^{2+} were explored using multiple complementary techniques including X-ray diffractometry (XRD), X-ray fluorescence (XRF), and scanning electron microscope energy dispersive spectrometry (SEM-EDS).

2. Materials and methods

2.1. Materials

The PR was from Guizhou, China. It was pulverized and sieved into particle sizes of <80 μm. The PR was used as seed crystals. Six stock solutions containing F^-, PO_4^{3-}, Ca^{2+}, Cu^{2+}, Zn^{2+}, Pb^{2+}, and NOM (natural organic matter) were prepared by dissolving NaF, $NaH_2PO_4{\cdot}2H_2O$, $CaCl_2{\cdot}2H_2O$, $CuCl_2{\cdot}2H_2O$, $ZnCl_2$, $PbCl_2$, and humic acid sodium salt into distilled water, respectively. All of the experiments were performed at room temperature (25°C ± 2°C).

Humic acid sodium salt used in this study was purchased from Sigma-Aldrich Co. (St. Louis, USA). All of the other chemicals were of analytical grade and purchased from the Sinopharm Chemical Reagent Co., Ltd. (Shanghai, China) and the Tianjin Kermel Chemical Reagent Co. Ltd. (Tianjin, China).

2.2. Conditional experiments procedures

2.2.1. Effect of Ca:P:F mole ratio

First, 0.25 mM NaF solutions with different concentrations of Cu^{2+} (0, 5, and 10 mg L^{-1}) were put into polymethyl methacrylate beakers, and 100 g seed crystals were put into the solution. The mixtures were placed under a coagulation test stirrer (MY3000-6, MeiYu, China) and agitated at 400 r min^{-1} for 2 min. Then, NaH_2PO_4 and $CaCl_2$ solutions were added in succession with Ca:P:F molar ratios of 5:3:1, 8:4:1, 12:6:1, and 20:10:1. Finally, the solutions were stirred at 100 r min^{-1} for 1 h. The resulting supernatants were filtered through a 0.45 μm membrane filter for analysis.

2.2.2. Reaction time

The experiments were performed with a Ca:P:F molar ratio of 12:6:1 with Cu^{2+} masses of 0, 5, and 10 mg L^{-1}. The experimental processes were consistent with the experiments above. The changes in F^-, $P–PO_4$, Ca^{2+}, and pH were recorded with reaction time.

2.2.3. Effect of HA

First, 100 g of seed crystals were added to the solutions that consisted of 0.25 mM NaF and 5, 10, 15, 20, 25, and 30 mg L^{-1} of HA. The Ca:P:F molar ratio was kept at 12:6:1. The experimental procedures were roughly the same with previous ones. The resulting supernatants were also filtered through a 0.45 μm membrane filter for the component analysis. These experiments were performed at different concentrations of Cu^{2+} (0, 5, and 10 mg L^{-1}).

2.2.4. Reuse of PR

The experiments were performed with a Ca:P:F molar ratio of 12:6:1 and 0, 5, and 10 mg L^{-1} of Cu^{2+}. The experimental process was the same as that of the reaction in Section 2.2.1. The PR samples were flushed with distilled water eight times and dried in the oven at 110°C for 12 h. The dried materials were reused as seed crystals in the experiments; these procedures were conducted 10 times.

2.2.5. Artificial groundwater experiments

The groundwater used in these experiments was referred to the mine-impacted groundwater at the Phoenix mine (Nevada, USA) [25]. The concentrations of ions in the artificial groundwater were as follows: F^- (2.88 mg L^{-1}), Ca^{2+} (300 mg L^{-1}), Cu^{2+} (9.45 mg L^{-1}), Pb^{2+} (0.122 mg L^{-1}), and Zn^{2+} (10.6 mg L^{-1}). The pH value of artificial groundwater was 4.2; it was adjusted with hydrochloric acid. Seed crystals PR (100 g) were put into 1 L of the artificial groundwater. The mixture was placed under a coagulation test stirrer and agitated at 400 rpm for 2 min. Next, NaH_2PO_4 stock solution was added successively with P:F molar ratios of 5:1, 6:1, 8:1, 10:1, 12:1, and 15:1. The remaining steps follow the previously mentioned experiments.

2.3. Analysis

The concentrations of F^-, $P–PO_4$, and Ca^{2+} in the resulting supernatant were tested using ion chromatography

(IC; ICS-1100; Thermo, USA). These samples were filtered with a 0.22 μm membrane filter before testing. The concentrations of Zn^{2+}, Pb^{2+}, and higher concentrations of Cu^{2+} (0.001–0.05 mg L^{-1}) were measured using atomic absorption (AA, ICE-3300, USA). The lower concentrations of Cu^{2+} (Cu^{2+} < 0.001 mg L^{-1}) were measured using inductive coupled plasma-atomic emission spectroscopy (ICP-AES, ELANDRC-E; USA). The pH values were determined with a pH meter (STARTER 3100 pro; OHAUS, USA). All of the samples to be tested were performed in triplicate, and the mean (±SD) is reported.

3. Results and discussion

3.1. Characteristics of PR

The components of the PR are presented in Table 1. The XRD data of the raw PR are presented in Fig. 1. The PR was composed of $Ca_{10}(PO_4)_6F_2$ and small amounts of $CaCO_3$, SiO_2, and $FePO_4$. The SEM-EDS image shows that the raw PR were irregular and smooth (Fig. 2). The elemental content table also indicated that there were elements forming the $Ca_5(PO_4)_3F$, $CaCO_3$, and SiO_2 that were the main compositions of PR.

3.2. Effect of Ca:P:F molar ratio

The residual F^- concentration could not reach the drinking water quality standard (F^- < 1.0 mg L^{-1}) when the Ca:P:F molar ratios were 5:3:1 and 8:4:1 (Fig. 3). However, the residual F^- concentration could be satisfied when Ca:P:F molar ratios were 12:6:1, 16:8:1, and 20:10:1. The pH values were 6–8 at any Ca:P:F molar ratios. The residual P-PO_4 is maintained at a very low and stable value. The concentration of residual Ca^{2+} increased with increasing Ca:P:F molar ratios. The residual Ca^{2+} values steadily increase as the Cu^{2+} concentration increases. The Cu^{2+} ions are almost completely removed at all scales. Thus, the Cu^{2+} concentration met the drinking water standard (Cu^{2+} < 1.0 mg L^{-1}).

Fig. 3c shows that the concentration of residual Ca^{2+} was greater than the initial Ca^{2+} concentration when the Cu^{2+} concentration was 10 mg L^{-1} with a Ca:P:F ratio of 5:3:1. There are several reasons for this phenomenon: (1) PR was composed of a small amount of $CaCO_3$ (Fig. 1). $CaCO_3$ was partially dissolved, as shown in the XRF results of PR (Table 1), and the weight portions of Ca^{2+} in the spent PR were smaller than that in the raw PR. (2) The Cu^{2+} coprecipitated with $Ca_{10}(PO_4)_6F_2$ and led to the formation of $Ca_{10-x}(Cu)_x(PO_4)_6F_2$ (x = 0.05–2.0) [24], which leads to a reduction of Ca^{2+} consumed. This phenomenon could also be supported by the SEM-EDS results (Figs. 2c and d). The Cu^{2+} appeared on the surface of the spent seed crystals. These observations explain why the residual Ca^{2+} was larger than the initial Ca^{2+}.

Importantly, both raw and spent PR were composed of $Ca_{10}(PO_4)_6F_2$, $CaCO_3$, SiO_2, and $FePO_4$; no Cu-containing mineral was found in XRD patterns of spent PR (Fig. 1). Former researchers showed similar results that XRD pattern of Cu^{2+} substituted fluorapatite $Ca_{10-x}(Cu)_x(PO_4)_6F_2$. This showed no differences with that of $Ca_{10}(PO_4)_6F_2$ in the peak positions except that the replacement of Ca^{2+} by Cu^{2+} decreased both the lattice parameters a and c of substituted fluorapatite phases slightly [21,24].

3.3. Crystallization kinetics

The kinetic experiments were performed with a Ca:P:F of 12:6:1 at different Cu^{2+} concentrations. The changes of F^-, P–PO_4, Ca^{2+}, and pH with the reaction time are shown in Fig. 4. The concentration of F^- rapidly fell to 1.0 mg L^{-1} after the $CaCl_2$ stock solution was added into the solution at different Cu^{2+} concentrations; the concentration of F^- remained below

Table 1
Chemical composition of PR

Constituent	Value (wt.%)			
	Raw PR	Spent PR (Cu^{2+} 0 mg L^{-1})	Spent PR (Cu^{2+} 5 mg L^{-1})	Spent PR (Cu^{2+} 10 mg L^{-1})
Ca	59.01	54.11	54.07	54.43
P	27.73	26.32	26.61	26.74
F	1.18	1.10	1.21	1.17
Cu	–	–	0.04	0.12
Na	0.29	0.27	0.27	0.28
Mg	0.78	0.65	0.65	0.64
Al	0.98	2.08	2.08	2.01
Si	5.54	6.95	7.06	6.98
S	1.66	2.97	3.05	3.13
K	0.29	0.39	0.37	0.34
Ti	0.13	0.19	0.17	0.17
Mn	0.13	0.17	0.17	0.18
Fe	2.03	3.60	3.60	3.64
Sr	0.08	0.08	0.08	0.09
Ba	0.17	1.12	0.57	0.08

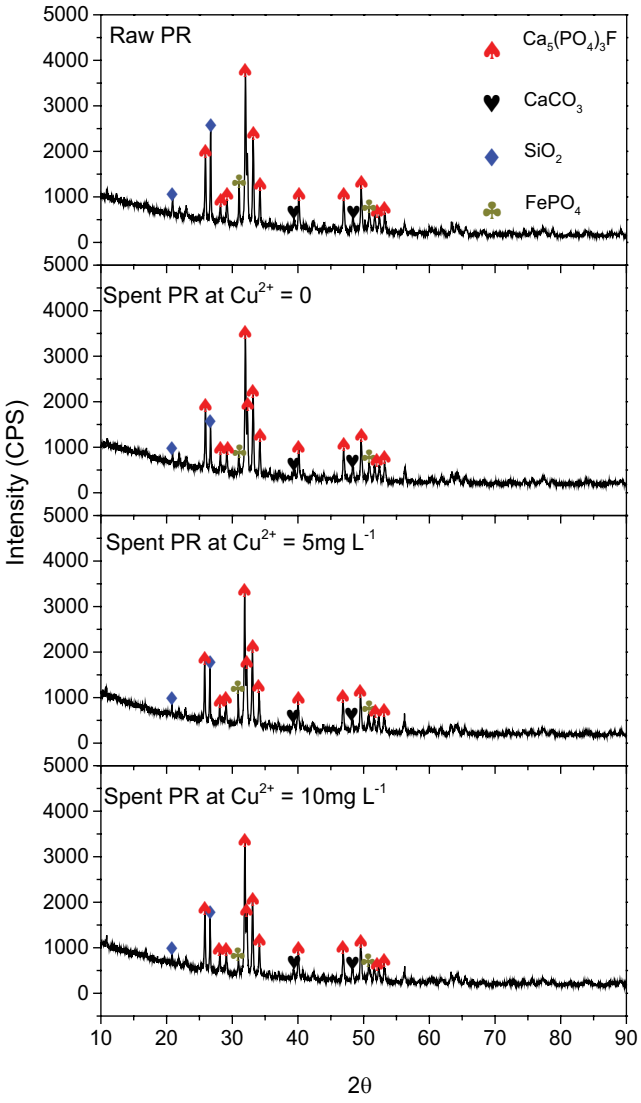

Fig. 1. XRD pattern of seed crystal after the fifth reuse: (a) raw PR, (b) spent PR at Cu^{2+} = 0 mg L^{-1}, (c) spent PR at Cu^{2+} = 5 mg L^{-1}, and (d) spent PR at Cu^{2+} = 10 mg L^{-1}.

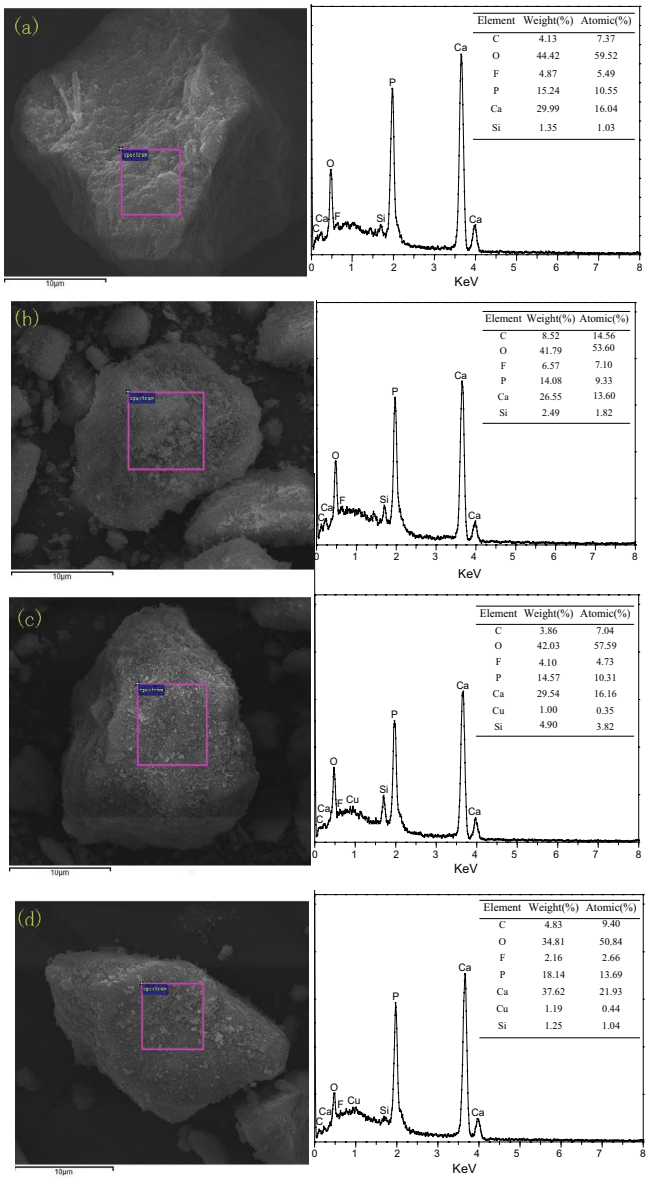

Fig. 2. SEM-EDS images and corresponding elemental compositions of seed crystal after the fifth reuse at 10,000x: (a) raw PR, (b) spent PR at Cu^{2+} = 0 mg L^{-1}, (c) spent PR at Cu^{2+} = 5 mg L^{-1}, and (d) spent PR at Cu^{2+} = 10 mg L^{-1}.

1.0 mg L^{-1} for the following 1 h. The trends of P–PO_4 and Ca^{2+} concentrations are consistent with that of F^-. The similar tendencies of F^-, P–PO_4, and Ca^{2+} indicate that these three substances are removed synchronously, which indirectly show the formation of the $Ca_{10}(PO_4)_6F_2$. The pH of the solution has no significant change and the values remain neutral. The residual Cu^{2+} concentrations were sharply decreased to the BLD (below limited detection) value during mixing within the first 2 min at Cu^{2+} concentrations of 5 and 10 mg L^{-1}. The results are not shown here. The Cu^{2+} was removed by co-precipitation with $Ca_{10}(PO_4)_6F_2$ via the formation of $Ca_{10-x}(Cu)_x(PO_4)_6F_2$ (x = 0.05–2.0).

Here, induced crystallization was determined by surveying the change of the F^- concentration and pH value as the crystallization formed. Fig. 4 shows that the pH value stabilizes at about 7 with more than half of the phosphates existing as HPO_4^{2-} in the solution at this pH value.

The amount of the crystallization may be calculated as the reduction of F^- as described in the following formula:

$$10Ca^{2+} + 6HPO_4^{2-} + 2F^- \rightarrow Ca_{10}(PO_4)_6F_2 + 6H^+ \quad (1)$$

The pH change was related to the decrease of the concentration of F^-, and the rate of $Ca_{10}(PO_4)_6F_2$ is connected to change of the F^- concentration. The relationship can be expressed as follows:

$$-\frac{d[F^-]}{dt} = 6\frac{d[H^+]}{dt} \quad (2)$$

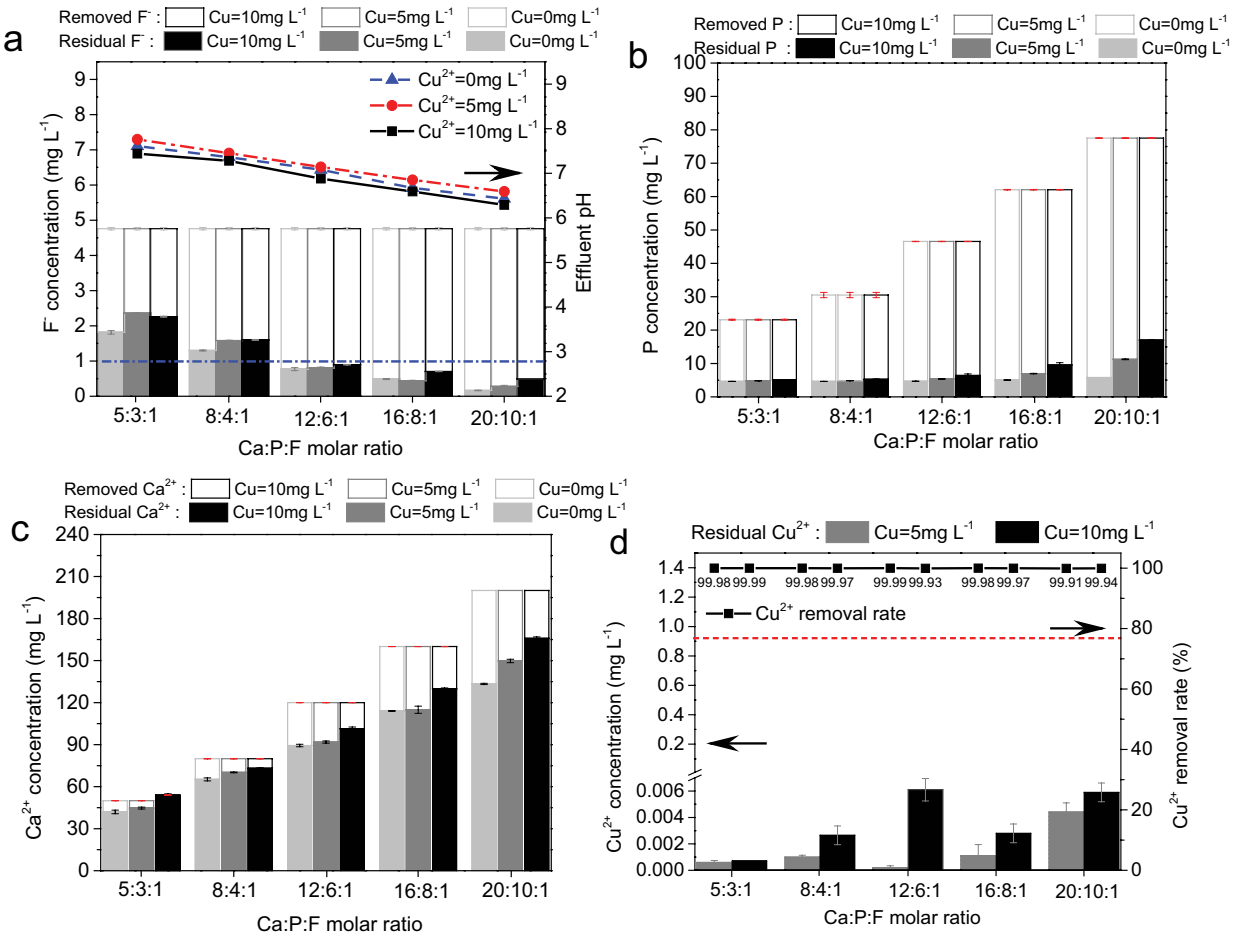

Fig. 3. Effect of Ca:P:F molar ratio on the residual concentrations of (a) F^- and final pH, (b) P–PO_4, (c) Ca^{2+}, and (d) Cu^{2+}. The blue and red dotted line denotes the Chinese acceptable F^- (<1.0 mg L^{-1}) and Cu^{2+} (<1.0 mg L^{-1}) standards for drinking water, respectively.

The relation between Eq. (2) and pH of the solution was studied via the kinetics of the struvite crystalization [26]. The left-hand side of Eq. (2) may be written as:

$$-\frac{d[F^-]}{dt} = k_F[F^-] \quad \text{or} \quad -\frac{d[F^-]}{[F^-]} = k_F dt \tag{3}$$

Similarly, the right-hand side of Eq. (2) can be expressed as:

$$\frac{d[H^+]}{dt} = k_H[H^+] \quad \text{or} \quad \frac{d[H^+]}{[H^+]} = k_H dt \tag{4}$$

The following formula can be obtained from the combination of Eqs. (3) and (4):

$$-\frac{d[F^-]}{[F^-]} = 6\frac{d[H^+]}{[H^+]} \tag{5}$$

It is known that pH = —log [H^+], so Eq. (5) can be integrated to yield

$$-\int_0^t \frac{d[F^-]}{[F^-]} = 6\int_0^t \frac{d[H^+]}{[H^+]} \tag{6}$$

Then,

$$\ln[F^-]^t = \ln[F^-]^0 - 6\ln\frac{[H^+]^t}{[H^+]^0} \tag{7}$$

$$\ln[F^-]^t = \ln[F^-]^0 - 6\ln\frac{[10^{-pH^t}]}{[10^{-pH^0}]} \tag{8}$$

or

$$\ln[F^-]^t = \exp\left[\ln[F^-]^0\right] - \left[\frac{10^{-pH^t}}{10^{-pH^0}}\right]^6 \tag{9}$$

$$[P]^t = \exp\left[\ln[P]^0\right] - \left[\frac{10^{-pH^t}}{10^{-pH^0}}\right] \tag{10}$$

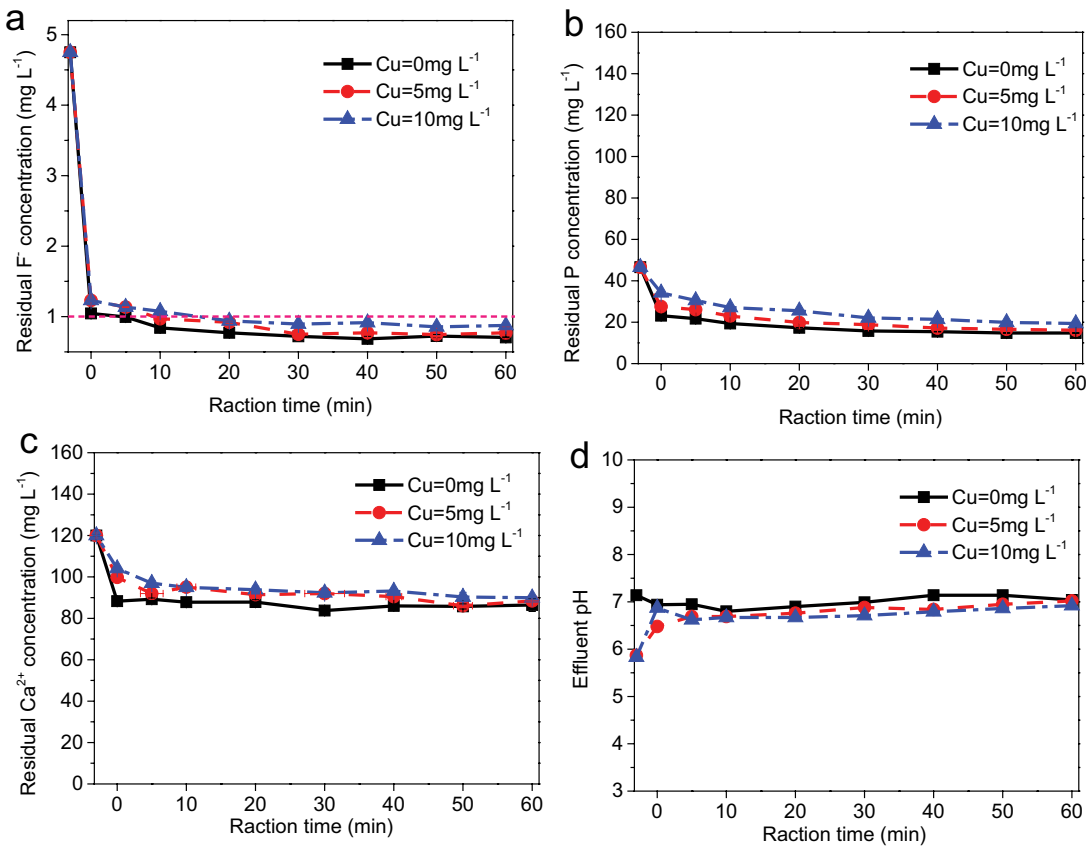

Fig. 4. Effect of contact time on the residual concentrations of (a) F^-, (b) $P–PO_4$, (c) Ca^{2+}, and (d) final pH. The red dotted line denotes the Chinese acceptable F^- (<1.0 mg L^{-1}) standards for drinking water.

The concentration of F^- in the solution during the reaction is calculated by Eq. (9). In particular, the concentration of $P–PO_4$ in the resulting solution is calculated in accordance with the method of calculating F^- as shown in Eq. (10). Next, the kinetic constants of the $Ca_{10}(PO_4)_6F_2$ crystallization were fitted to a suitable kinetic model. In this study, we used the pseudo-first-order and the pseudo-second-order kinetic models to show the calculated results. The linear form of the expression of the pseudo-first-order kinetics Eq. (11) and the pseudo-second-order kinetics Eq. (12) were written as follows:

$$\ln c = -kt + \ln c_0 \tag{11}$$

$$\frac{1}{c_0} = -kt + \frac{1}{c} \tag{12}$$

where c = [F^-] at any time, t (molar), c_0 = [F^-] at start time (molar), k = reaction rate constant, (1/min (the pseudo-first-order kinetic), mg L^{-1} min^{-1} (the pseudo-second-order kinetic)), t = reaction time (min).

The results of the fitting are expected to be a straight line: This would demonstrate that the experimental results can be fitted with these two models.

The pseudo-first-order and the pseudo-second-order kinetic fittings of F^- and $P–PO_4$ carried out at various Cu^{2+} concentrations are described in Fig. 5. The changes in F^- and $P–PO_4$ concentrations are a better fit with the pseudo-first-order kinetics at 0 mg L^{-1} Cu^{2+}. This is because the R^2 of the pseudo-first-order is larger than that of the pseudo-second-order kinetics. When Cu^{2+} was 5 mg L^{-1}, the change in F^- and $P–PO_4$ concentrations both fit the pseudo-second-order kinetics. When Cu^{2+} was 10 mg L^{-1}, the variation of F^- and $P–PO_4$ concentrations both nicely fitted the pseudo-second-order kinetics. The rate constant of F^- will first increase and then decrease with increasing Cu^{2+} concentrations with both kinetic fittings. The pseudo-second-order kinetics was a better fit than the pseudo-first-order kinetics for residual $PO_4–P$. The rate constant of $P–PO_4$ with pseudo-second-order kinetics fitting decreased slowly with increasing Cu^{2+} concentration. Because the seed crystals used in this study contained $CaCO_3$, the Ca^{2+} would simultaneously participate in the dissociation and precipitation of $CaCO_3$ and $Ca_{10}(PO_4)_6F_2$ so that the change of the Ca^{2+} concentration cannot be fitted with any kinetics model. Those results are not shown here.

3.4. Effect of natural organic matter

HA is a common macromolecular organic compound existing in natural water so the effects of HA on the changes of F^-, $P–PO_4$, Ca^{2+}, pH, and Cu^{2+} with a Ca:P:F ratio of 12:6:1 were studied (Fig. 6). The F^- concentration was lower than 1.0 mg L^{-1} at any HA concentration. The pH values were

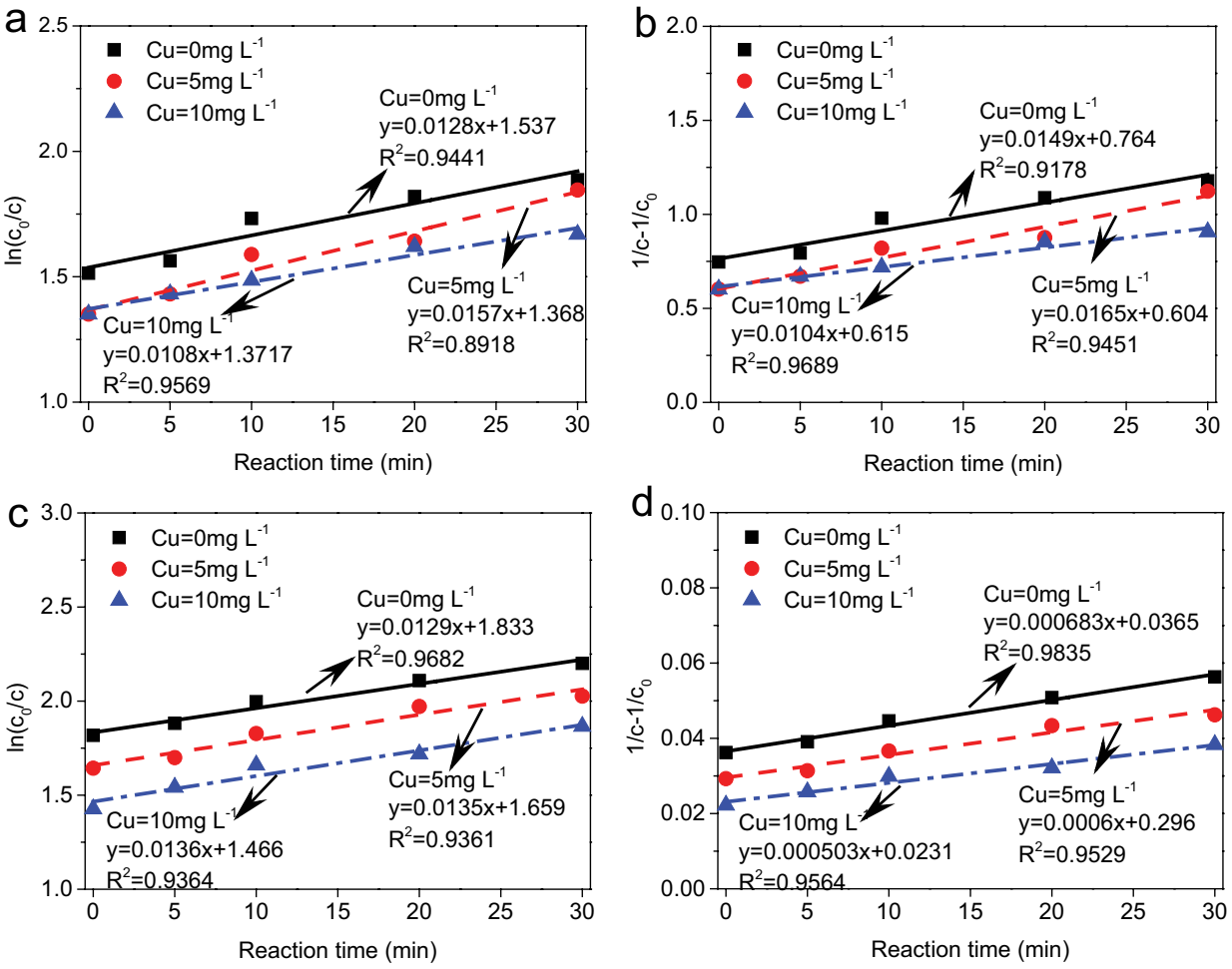

Fig. 5. Kinetic fitting: (a) the first-order kinetics of F^-, (b) the second-order kinetics of F^-, (c) the first-order kinetics of P, and (d) the second-order kinetics of P.

stable and neutral at all of the conditions. The removal rates of P–PO_4 were not significantly changed with changes of HA concentration. They increased slightly with increasing Cu^{2+} concentration. The change trend in the removal rate of Ca^{2+} is consistent with that of the removal rate of P–PO_4. In the series of experiments, Cu^{2+} was almost completely removed at any initial Cu^{2+} concentration, and the values satisfy the water quality standard (Cu^{2+} < 1.0 mg L^{-1}).

3.5. Reuse of PR

The residual F^- concentration increased with increasing cycle numbers and initial Cu^{2+} concentrations (Fig. 7). The final pH decreased gradually from 7.0 to 5.5. The removal rate of P–PO_4 increased with both an increase in initial Cu^{2+} concentration and the cycle numbers. The residual Ca^{2+} concentrations have similar change trends with the residual P–PO_4. Without introducing Cu^{2+}, the residual F^- concentrations at cycles 1–10 were all less than 1.0 mg L^{-1}. The F^- was removed by the formation of $Ca_{10}(PO_4)_6F_2$ as described [27]. The XRD result showed that $Ca_{10}(PO_4)_6F_2$ was the main component of the raw PR (Fig. 1). The surface of the PR seed crystal nicely matched the $Ca_{10}(PO_4)_6F_2$ crystal to be formed. This showed a surface-catalytic effect [28]. Thus, the induced crystallization tended to form a structurally continuous coating on the seed crystals grain.

When the initial concentration of Cu^{2+} increased to 5.0 mg L^{-1}, the residual F^- was above 1.0 mg L^{-1} after the sixth round. The concentrations of Cu^{2+} were less than 1.0 mg L^{-1}. When the initial Cu^{2+} concentration reached 10 mg L^{-1}, the residual F^- was more than 1.0 mg L^{-1} after only four rounds. The level of Cu^{2+} was beyond 1.0 mg L^{-1} after the seventh round. Notably, at cycle 10, the residual F^-, P–PO_4 and Ca^{2+} at Cu^{2+} 5 and 10 mg L^{-1} were still supersaturated with $Ca_{10}(PO_4)_6F_2$ after the induced crystallization process (Fig. 7). The retarding effect of Cu^{2+} on the crystallization of $Ca_{10}(PO_4)_6F_2$ might be because Cu obstructs the deposition of lattice ion Ca on the surface of PR [28], that is, the crystallization of $Ca_{10}(PO_4)_6F_2$, Cu^{2+} was a foreign constituent. The co-precipitation of Cu^{2+} with $Ca_{10}(PO_4)_6F_2$ on the PR surfaces forms $Ca_{10-x}(Cu)_x(PO_4)_6F_2$ (x = 0.05–2.0) [24]. The newly formed $Ca_{10-x}(Cu)_x(PO_4)_6F_2$ coated surface do not match the $Ca_{10}(PO_4)_6F_2$ matrix. Thus, it slows down the growth kinetics of $Ca_{10}(PO_4)_6F_2$. As a result, F^-, P–PO_4 and Ca^{2+} remained in the system remained in the system although the solution was still supersaturated with $Ca_{10}(PO_4)_6F_2$.

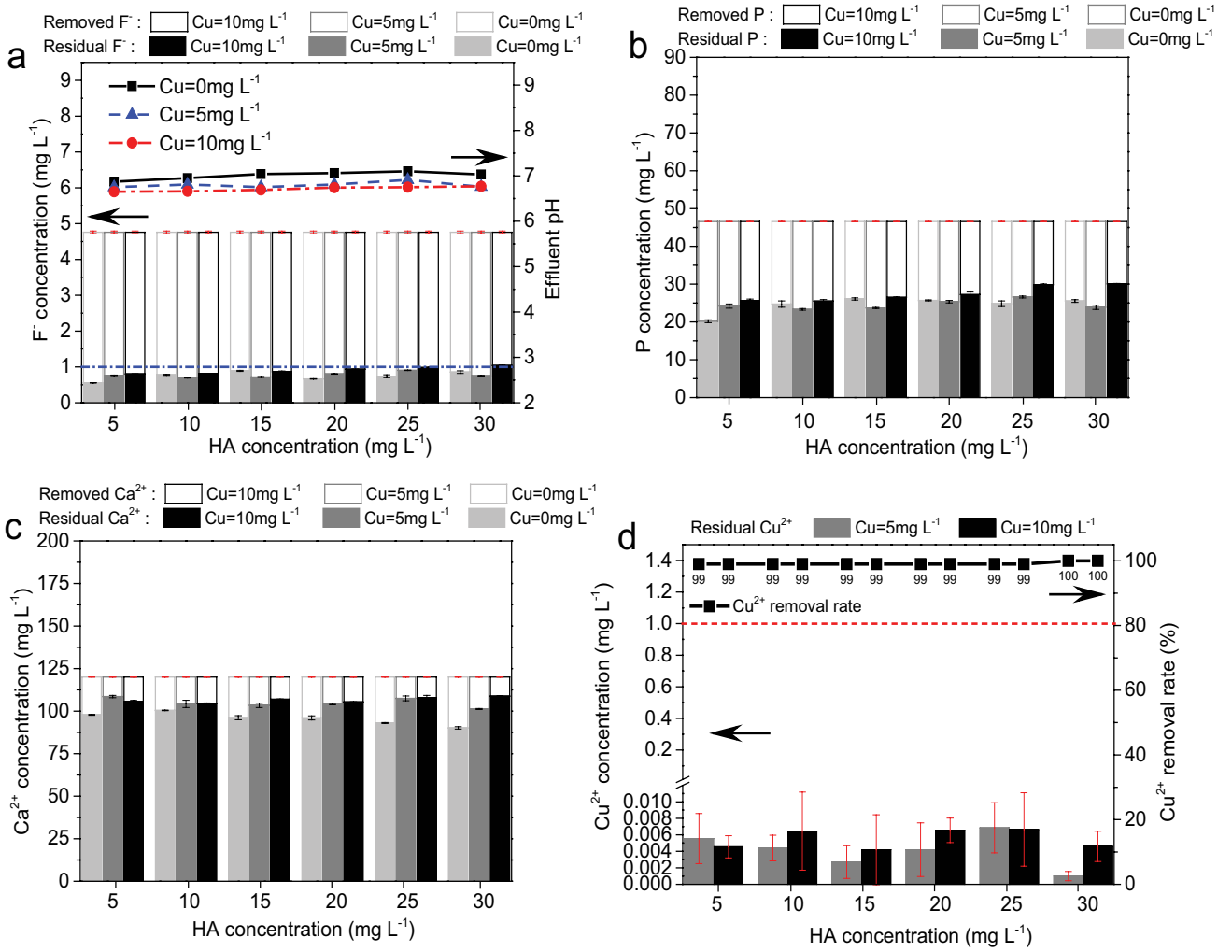

Fig. 6. Effect of HA concentration on the residual concentrations of (a) F^- and final pH, (b) P–PO_4, (c) Ca^{2+}, and (d) Cu^{2+}. The blue and red dotted line denotes the Chinese acceptable F^- (<1.0 mg L^{-1}) and Cu^{2+} (<1.0 mg L^{-1}) standards for drinking water, respectively.

3.6. Simultaneous removal of F^-, Cu^{2+}, Zn^{2+}, and Pb^{2+}

Mining affects the environment, including groundwater, although the routes of pollution can vary. Polluted aquifers act as long-term pollution sources to the surrounding environment even after the mining activities have ended [29]. The groundwater surrounding gold mines, copper mines, and polymetallic mines is often contaminated with aluminium, iron, nickel, zinc, copper, lead, etc. [25,29,30]. Thus, artificial groundwater experiments were conducted here.

Artifical groundwater was used along with groundwater near the Phoenix mine in the Copper Canyon district. The concentrations of ions in the artificial groundwater were F^- (2.88 mg L^{-1}), Ca^{2+} (300 mg L^{-1}), Cu^{2+} (9.45 mg L^{-1}), Pb^{2+} (0.122 mg L^{-1}), and Zn^{2+} (10.60 mg L^{-1}), and the pH was 4.2. The concentration of Ca^{2+} is about 50 fold higher than F^- so no extra Ca^{2+} was added. Fig. 8 shows that the residual F^- is below 1.0 mg·L^{-1} with P:F ratios of 8:1, 10:1, 12:1, and 15:1. The removal rate of F^- increased with increase in the P:F molar ratio. The final pH values were 6–8 and decreased gradually. The removal rate of P–PO_4 decreased with increasing P:F molar ratios. The residual Ca^{2+} slightly decreased as the molar ratio of P:F increased. The heavy metals Cu^{2+}, Zn^{2+}, and Pb^{2+} were almost completely removed at every condition (Table 2).

4. Conclusions

We evaluated the simultaneous removal of F^- and Cu^{2+} by induced crystallization using phosphate rock as a seed crystal. The resulting concentrations of F^- and Cu^{2+} were below the water quality limit (both 1.0 mg L^{-1}) when the Ca:P:F molar ratios were 12:6:1, 16:8:1, and 20:10:1. The kinetic characteristics of F^- removal fit the pseudo-second-order model, and the reaction rate constants decreased with increasing Cu^{2+} concentrations. A high amount of Cu^{2+} was an obstacle to F^- removal. The retarding effect of Cu^{2+} on the removal of F^- can be explained as being due primarily to the obstruction by Cu^{2+} to the deposition of lattice ion Ca^{2+} on the surface of PR. Hence, this hindered the induced crystallization of $Ca_{10}(PO_4)_6F_2$. The concentration of HA (5–30 mg L^{-1}) does not have any negative impact on the removal of F^- and Cu^{2+}. When the artificial groundwater containing F^-, Cu^{2+}, Zn^{2+}, and

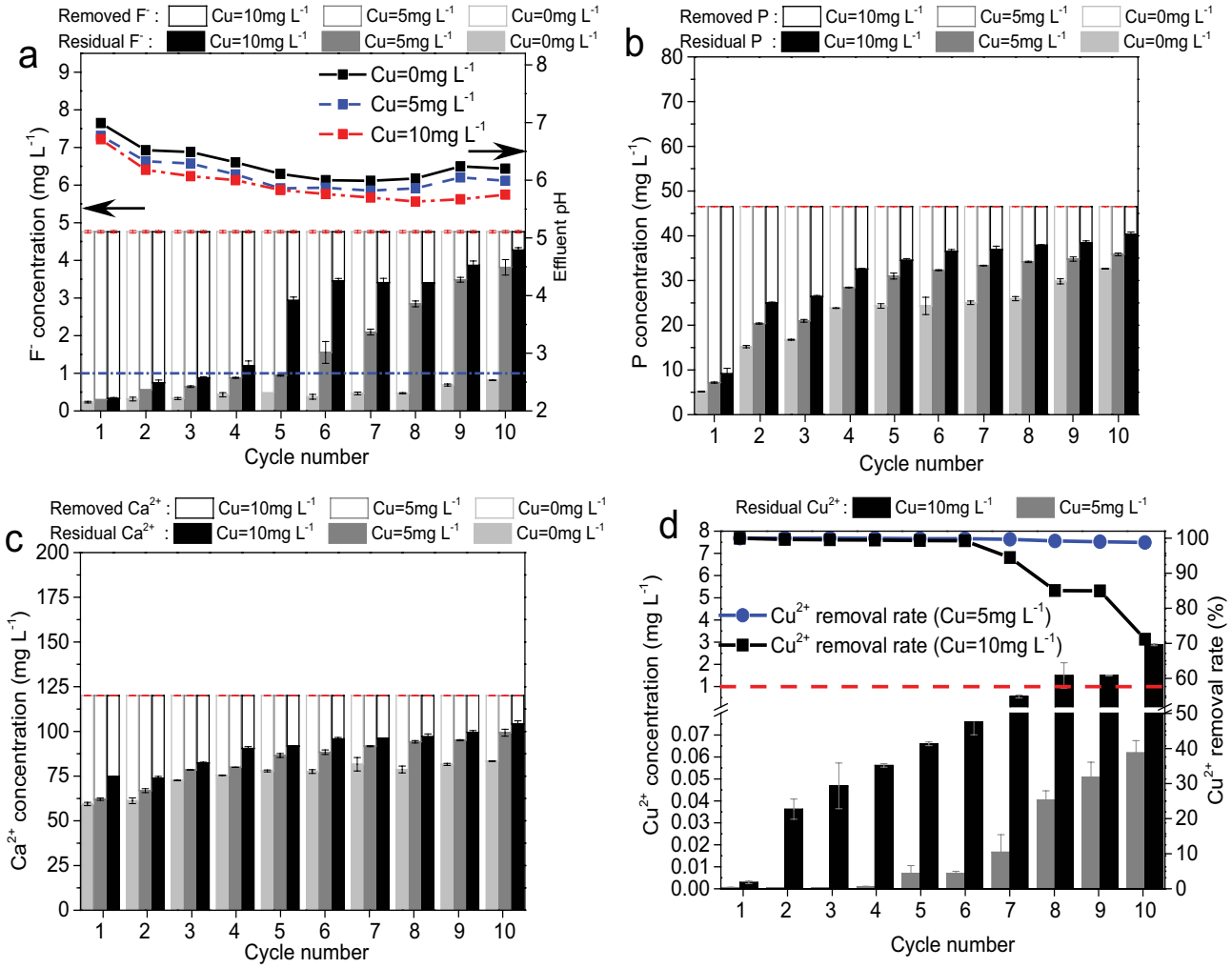

Fig. 7. Residual concentrations of (a) F^- and final pH, (b) P–PO_4, (c) Ca^{2+}, and (d) Cu^{2+} as well as removal rate. The blue and red dotted line denotes the Chinese acceptable F^- (<1.0 mg L^{-1}) and Cu^{2+} (< 1.0 mg L^{-1}) standards for drinking water, respectively.

Table 2
Residual concentrations of Cu^{2+}, Zn^{2+}, and Pb^{2+} with different P:F ratios

P:F proportion	3:1	6:1	8:1	10:1	12:1	15:1	WQS[b]
	Concentration (mg L^{-1})						
Cu^{2+}	0.0006	0.0007	0.0009	0.0003	0.0008	0.0015	1.0
Zn^{2+}	BLD[a]	BLD	BLD	BLD	BLD	BLD	1.0
Pb^{2+}	BLD	BLD	BLD	BLD	BLD	BLD	0.01

[a]Blow limited detection (Zn^{2+}: <0.05 mg L^{-1}, Pb^{2+}: <0.001 mg L^{-1}).
[b]Water quality standard.

Pb^{2+} ions was treated by this process, the residual concentrations of these ions were all below the Chinese drinking water guidelines (P:F molar ratio above 6:1). This induced crystallization technology could be used in groundwater application for the removal of multiple contaminants including F^- and typical heavy metal ions.

Acknowledgments

This work was supported by the National Natural Science Foundation of China (Grant No. 51308436), the National Key Research Program of China (Grant No. 2016YFC0400706), the Shaanxi Science & Technology Co-ordination & Innovation

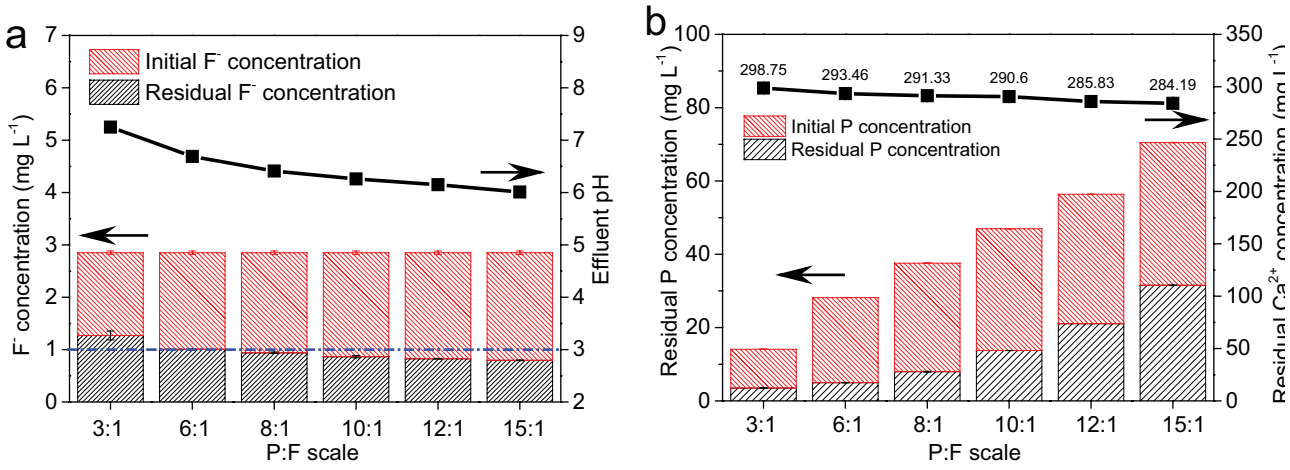

Fig. 8. Effect of P:F molar ratio on the residual concentrations of (a) F^- and final pH, (b) P–PO_4 and Ca^{2+}. The blue dotted line denotes the Chinese acceptable F^- (<1.0 mg L^{-1}) standards for drinking water.

Project (Grant No. 2015KTCL-03-15), and the National Natural Science Foundation of China (Grant No. 51278404).

References

[1] MOHC (The Minister of Health of the People's Republic of China), Standard for Drinking Water Quality, GB5749-2006. Standards Press of China, China, 2006.
[2] J. Wilhelmi, R. Bopp, R. Brown, J. Cherwinka, J. Cummings, E. Dale, M. Diwan, J. Goett, R.W. Hackenburg, J. Kilduff, L. Littenberg, G.S. Li, X.N. Li, J.C. Liu, H.Q. Lu, J. Napolitano, C. Pearson, N. Raper, R. Rosero, P. Stoler, Q. Xiao, C.G. Yang, Y. Yang, M. Yeh, The water purification system for the Daya Bay Reactor Neutrino Experiment, J. Water Process Eng., 5 (2015) 127–135.
[3] A.K. Misra, Influence of stone quarries on groundwater quality and health in Fatehpur Sikri, India, Int. J. Sustain. Built Environ., 2 (2013) 73–88.
[4] H.-m. Cai, G.-j. Chen, C.-y. Peng, Z.-z. Zhang, Y.-y. Dong, G.-z. Shang, X.-h. Zhu, H.-j. Gao, X.-c. Wan, Removal of fluoride from drinking water using tea waste loaded with Al/Fe oxides: a novel, safe and efficient biosorbent, Appl. Surf. Sci., 328 (2015) 34–44.
[5] M. Vithanage, P. Bhattacharya, Fluoride in the environment: sources, distribution and defluoridation, Environ. Chem. Lett., 13 (2015) 131–147.
[6] X. Xu, Q. Li, H. Cui, J. Pang, L. Sun, H. An, J. Zhai, Adsorption of fluoride from aqueous solution on magnesia-loaded fly ash cenospheres, Desalination, 272 (2011) 233–239.
[7] Y. Ma, F. Shi, X. Zheng, J. Ma, C. Gao, Removal of fluoride from aqueous solution using granular acid-treated bentonite (GHB): batch and column studies, J. Hazard. Mater., 185 (2011) 1073–1080.
[8] C.J. Huang, J.C. Liu, Precipitate flotation of fluoride-containing wastewater from a semiconductor manufacturer, Water Res., 33 (1999) 3403–3412.
[9] M.D.G. de Luna, Warmadewanthi, J.C. Liu, Combined treatment of polishing wastewater and fluoride-containing wastewater from a semiconductor manufacturer, Colloids Surf., A, 347 (2009) 64–68.
[10] C. Su, Y. Wang, X. Xie, J. Li, Aqueous geochemistry of high-fluoride groundwater in Datong Basin, Northern China, J. Geochem. Explor., 135 (2013) 79–92.
[11] A. Narsimha, V. Sudarshan, Data on fluoride concentration levels in semi-arid region of Medak, Telangana, South India, Data Brief, 16 (2018) 717–723.
[12] M. Mirzabeygi, M. Yousefi, H. Soleimani, A.A. Mohammadi, A.H. Mahvi, A. Abbasnia, The concentration data of fluoride and health risk assessment in drinking water in the Ardakan city of Yazd province, Iran, Data Brief, 18 (2018) 40–46.
[13] S.K. Gautam, C. Maharana, D. Sharma, A.K. Singh, J.K. Tripathi, S.K. Singh, Evaluation of groundwater quality in the Chotanagpur plateau region of the Subarnarekha river basin, Jharkhand State, India, Sustain. Water Quality Ecol., 6 (2015) 57–74.
[14] M.A. Alghobar, S. Suresha, Evaluation of metal accumulation in soil and tomatoes irrigated with sewage water from Mysore city, Karnataka, India, J. Saudi Soc. Agric. Sci., 16 (2017) 49–59.
[15] C.-M. Leung, J.J. Jiao, Heavy metal and trace element distributions in groundwater in natural slopes and highly urbanized spaces in Mid-Levels area, Hong Kong, Water Res., 40 (2006) 753–767.
[16] Z. Elouear, J. Bouzid, N. Boujelben, M. Feki, F. Jamoussi, A. Montiel, Heavy metal removal from aqueous solutions by activated phosphate rock, J. Hazard. Mater., 156 (2008) 412–420.
[17] J. Zheng, K.-h. Chen, X. Yan, S.-J. Chen, G.-C. Hu, X.-W. Peng, J.-g. Yuan, B.-X. Mai, Z.-Y. Yang, Heavy metals in food, house dust, and water from an e-waste recycling area in South China and the potential risk to human health, Ecotoxicol. Environ. Saf., 96 (2013) 205–212.
[18] M. Rosales, O. Coreño, J.L. Nava, Removal of hydrated silica, fluoride and arsenic from groundwater by electrocoagulation using a continuous reactor with a twelve-cell stack, Chemosphere, 211 (2018) 149–155.
[19] V.L. Dhadge, C.R. Medhi, M. Changmai, M.K. Purkait, House hold unit for the treatment of fluoride, iron, arsenic and microorganism contaminated drinking water, Chemosphere, 199 (2018) 728–736.
[20] N.N. Dil, M. Sadeghi, Free radical synthesis of nanosilver/gelatin-poly (acrylic acid) nanocomposite hydrogels employed for antibacterial activity and removal of Cu(II) metal ions, J. Hazard. Mater., 351 (2018) 38–53.
[21] M. Sarioglu, Ü.A. Atay, Y. Cebeci, Removal of copper from aqueous solutions by phosphate rock, Desalination, 181 (2005) 303–311.
[22] X. Cao, L.Q. Ma, D.R. Rhue, C.S. Appel, Mechanisms of lead, copper, and zinc retention by phosphate rock, Environ. Pollut., 131 (2004) 435–444.
[23] L. Deng, X. Zhang, T. Huang, J. Zhou, Investigation of fluorapatite crystallization in a fluidized bed reactor for the removal of fluoride from groundwater, J. Chem. Technol. Biotechnol., 94 (2019) 569–581.
[24] S. Shanmugam, B. Gopal, Copper substituted hydroxyapatite and fluorapatite: synthesis, characterization and antimicrobial properties, Ceram. Int., 40 (2014) 15655–15662.
[25] A. Davis, K. Heatwole, B. Greer, R. Ditmars, R. Clarke, Discriminating between background and mine-impacted

groundwater at the Phoenix mine, Nevada USA, Appl. Geochem., 25 (2010) 400–417.
[26] K.S. Le Corre, E. Valsami-Jones, P. Hobbs, S.A. Parsons, Kinetics of struvite precipitation: effect of the magnesium dose on induction times and precipitation rates, Environ. Technol., 28 (2007) 1317–1324.
[27] L. Deng, Y. Liu, T. Huang, T. Sun, Fluoride removal by induced crystallization using fluorapatite/calcite seed crystals, Chem. Eng. J., 287 (2016) 83–91.
[28] W. Stumm, J.J. Morgan, Aquatic Chemistry: Chemical Equilibria and Rates in Natural Waters, Wiley, New York, 1996.
[29] Y. Wang, R. Dong, Y. Zhou, X. Luo, Characteristics of groundwater discharge to river and related heavy metal transportation in a mountain mining area of Dabaoshan, Southern China, Sci. Total Environ., 679 (2019) 346–358.
[30] N.M. Burri, R. Weatherl, C. Moeck, M. Schirmer, A review of threats to groundwater quality in the anthropocene, Sci. Total Environ., 684 (2019) 136–154.